ACS OMEGA

Open Access

http://pubs.acs.org/journal/acsodf

Article

Exploring the Effect Mechanism of Alkyl Chain Lengths on the Tribological Performance of Ionic Liquids

Guowei Huang,* Li Sun, Luxing Li, Linlu Pei, Wangle Xue, Ruichao Wang, and Yifei Wang

Cite This: *ACS Omega* 2024, 9, 3184−3192

Read Online

ACCESS | Metrics & More | Article Recommendations | Supporting Information

ABSTRACT: In this work, four kinds of imidazole phosphate ionic liquids (ILs) with different anionic and cationic alkyl chain lengths were synthesized. The physicochemical properties and tribological performance of ILs were evaluated. The experimental results revealed that the tribological properties of ILs were positively correlated with the cationic chain length and negatively correlated with the anionic chain length. The effect mechanism can be summarized in two aspects: on the one hand, anions with shorter alkyl chain lengths possess stronger adsorption performance and better film forming ability on the friction pair surfaces, which makes the ILs form more robust and stable lubricating film; on the other hand, ILs with longer cationic alkyl chain lengths possess milder tribo-chemical reactions, which can effectively enhance the tribological performance and decrease the corrosion wear.

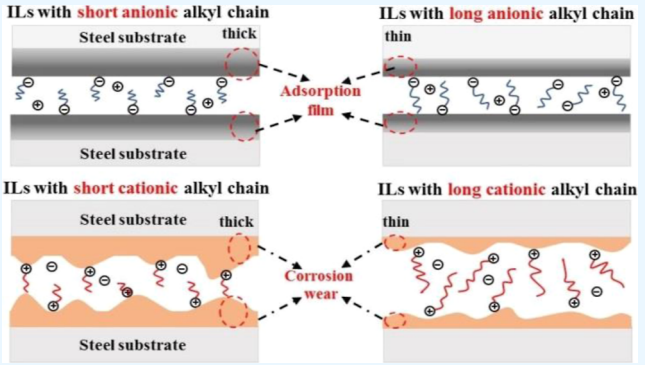

1. INTRODUCTION

With the continuous development of modern industry, there is an increasing number of severe working conditions for the employment of mechanical equipment, such as high loads, corrosion environments, and other harsh working environments.[1] Lubricating oil and grease can efficiently reduce friction and wear by avoiding direct contact of sliding pairs. However, most of them are prone to failure under a harsh environment.[2] Accordingly, a new type of synthetic lubricants is urgently required to enhance their tribological properties. Ionic liquids (ILs) as the new kind of high-performance lubricants and lubricant additives have been adopted since 2001 arising from their distinctive physicochemical properties, including negligible volatility, high heat resistance, nonflammability and favorable designability of molecular structures, and so forth.[3−6] Since then, ILs have entered the tribology researcher's field of vision and aroused extensive attention. A large quantity of ILs have been synthesized and their tribological properties have been explored.[7−10]

The friction-reducing and antiwear mechanisms of ILs have been extensively investigated and diffusely recognized as two aspects: one is the lubricating films formed by the anions and cations that adsorb on the sliding pair surfaces, and the other is the tribo-chemical reactions between ILs and substrate surfaces.[11−13] Meanwhile, ILs containing active elements (such as N and P) possess strong electronegativity and are liable to form chemical bonds with metal elements.[14−16] Therefore, alkyl imidazole ILs are extensively utilized as general lubricants for friction pairs owing to their remarkable corrosion resistance, high load-bearing properties, and tribological properties. Zheng et al. uncovered that guanidine-based ILs as the additives of di(2-ethylhexyl) phthalate and polyethylene glycogen (PEG200) can effectively enhance their wear resistance.[13] In addition, the synergistic effect of nitrogen and phosphorus can significantly promote the wear resistance performance of ILs. Liu et al. revealed that asymmetric tetra-alkyl-phosphonium ILs exhibit better tribological properties than traditional ILs.[4]

In our previous studies, the cations with longer alkyl chains of imidazolium-based ILs presented outstanding adsorption ability and tribological performance.[17] Pejaković et al. detected that the friction-reducing and antiwear properties of ILs are both promoted with the increase of the anionic alkyl chain length.[18] Previous research just simply interpreted the influence of cationic or anionic alkyl chain length on tribological properties, but the effect of anionic alkyl chain length and cationic and anionic alkyl chain lengths in the same system are rarely mentioned.

In this work, to further confirm the influence of anionic and cationic alkyl chain lengths on the tribological performance of ILs, four molecular structures of ILs are designed: long alkyl chain cation and long alkyl chain anion, long alkyl chain cation

Received: March 20, 2023
Accepted: June 13, 2023
Published: January 11, 2024

and short alkyl chain anion, short alkyl chain cation and long alkyl chain anion, and short alkyl chain cation and short alkyl chain anion. Through the evaluations of their tribological properties, adsorption behavior, and the analysis of wear scar surfaces, the influencing mechanism of anionic and cationic alkyl chain lengths on the tribological performance of ILs will be revealed more clearly and accurately.

2. EXPERIMENTAL SECTION

2.1. Materials and Synthesis of ILs. Di(6-methylheptyl) phosphate (99%), dibutyl phosphate (≥97%), *N*-methylimidazole (≥99%), 1-bromopropane (99%), and 1-bromodecane (98%) were purchased from J&K. Metallic sodium was bought from Sinopharm Chemical Reagent Co., Ltd. The sodium phosphates were lab-made. 1-Propyl-3-methyl-imidazole dibutyl phosphate ([PMIM][DBP]), 1-propyl-3-methyl-imidazole diisooctyl phosphate salt ([PMIM][DEHP]), 1-decyl-3-methyl-imidazole dibutyl phosphate sodium salt ([DMIM][DBP]), and 1-decyl-3-methyl-imidazole diisooctyl phosphate sodium salt ([DMIM][DEHP]) were synthesized according to the literature.[19] The synthetic route and molecular structures of the four ILs are illustrated in Figure 1. The infrared spectra of the ILs (in Figure S1) and the nuclear magnetic results proved the successful synthesis of the four ILs.

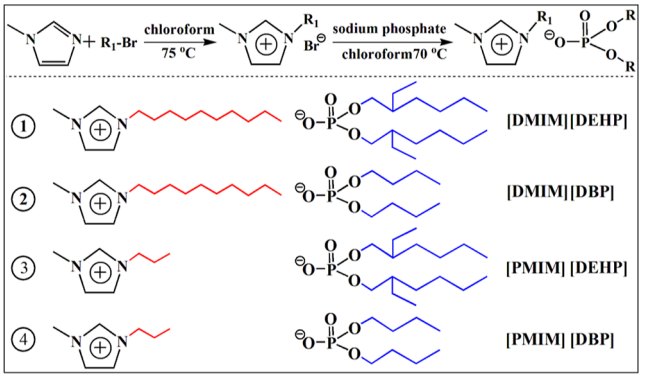

Figure 1. Synthetic process and corresponding molecular structures of the four ILs.

2.2. Characterization. A SVM3000 Stabinger viscometer was employed to measure kinematic viscosity of ILs at 25, 40, and 100 °C. STA 449 C Jupiter simultaneous thermogravimetry and differential scanning calorimetry were introduced to detect the thermostability of the four ILs from room temperature (RT) to 600 °C in a nitrogen atmosphere, and the heating rate was 10 °C/min. The corresponding testing results of the four ILs are depicted in Table 1 and Figure 2. The kinematic viscosity of [DMIM][DBP] and [PMIM][DEHP] are larger than those of [DMIM][DEHP] and [PMIM][DBP], and their decomposition temperatures are very close, approximately 200 °C.

A ball-on-disc SRV-IV oscillating reciprocating friction and wear test apparatus (the type of movement in tribometer: ASTMD 5707-098) was introduced to detect the tribological property. The material of the upper steel ball (ø 1.0 cm) and the lower steel disc (ø 2.4 × 0.79 cm) was AISI 52100 steel. The added amount of lubricant in each test was approximately 0.20 mL. The lubricant and wear debris were removed from the steel ball and the disc surfaces with alcohol cotton after the friction test; then the fresh lubricant was added to the untested site to start the new one. Test parameters in the experiments are described in Table 2.

Table 1. Kinematic Viscosities and Decomposition Temperatures of ILs

ILs	kinematic viscosity (mm^2/s)			viscosity index	decomposition temperature/°C
	25 °C	40 °C	100 °C		
[DMIM][DBP]	401.8	164.9	20.1	142	209.3
[DMIM][DEHP]	1032.1	426.1	32.6	111	228.9
[PMIM][DBP]	436.9	175.9	18.1	114	174.0
[PMIM][DEHP]	120.6	58.8	9.3	139	214.5

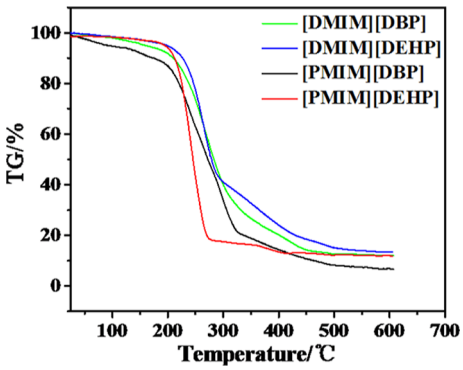

Figure 2. Thermal decomposition temperature curves of the four ILs.

Table 2. Experimental Parameters in the SRV-IV Test

amplitude (mm)	frequency (Hz)	load/contact pressure	test time	sliding distance
1	25	300 N/2.03 GPa	30 min	90 m
1	25	initial load: 50 N increase by 50 N/3 min	stop when stuck	

A JSM-5600LV scanning electron microscope (SEM) and a Micro-XAM 3D noncontact surface mapping profiler were introduced to detect the morphologies of wear scars and wear volumes separately. Before testing, the samples were cleaned with ethanol under ultrasound for three times to completely remove the ILs and wear debris. A DSA100 contact angle (CA) meter and DCAT 15 surface tension meter were separately utilized to measure the CAs of ILs on the surface of the steel blocks and their surface tensions. A PHI-5702 X-ray photoelectron spectrometer (XPS) and an energy dispersive spectrometer (EDS) were adopted to investigate the element composition and distribution of wear scar surfaces. The copper block corrosion tests of four ILs were performed. The specific steps and test results are as follows. The copper blocks (1.0 × 1.0 × 0.30 cm) were polished with 400-600-800-1200-1500 grade sandpaper in sequence. Subsequently, the polished metal blocks were cleaned ultrasonically three times with ethanol. The dried metal samples were immersed in the corresponding ILs. After being treated at 200 °C for 2 h, the metal blocks were taken out and the ILs on the surface were rinsed off with ethanol.

https://doi.org/10.1021/acsomega.3c01885
ACS Omega 2024, 9, 3184−3192

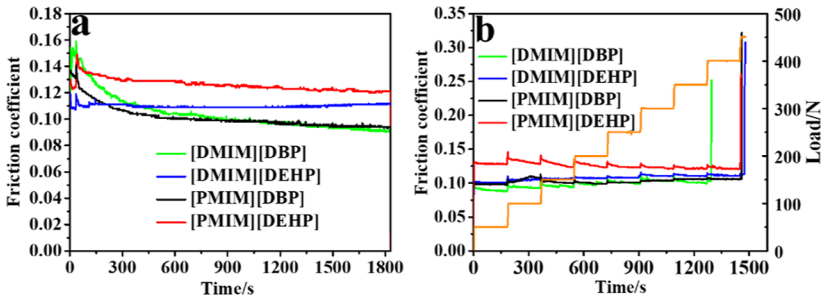

Figure 3. Friction coefficients of the four ILs under different test conditions: (a) 300 N, 25 Hz, and RT; (b) varying loads, 25 Hz and RT.

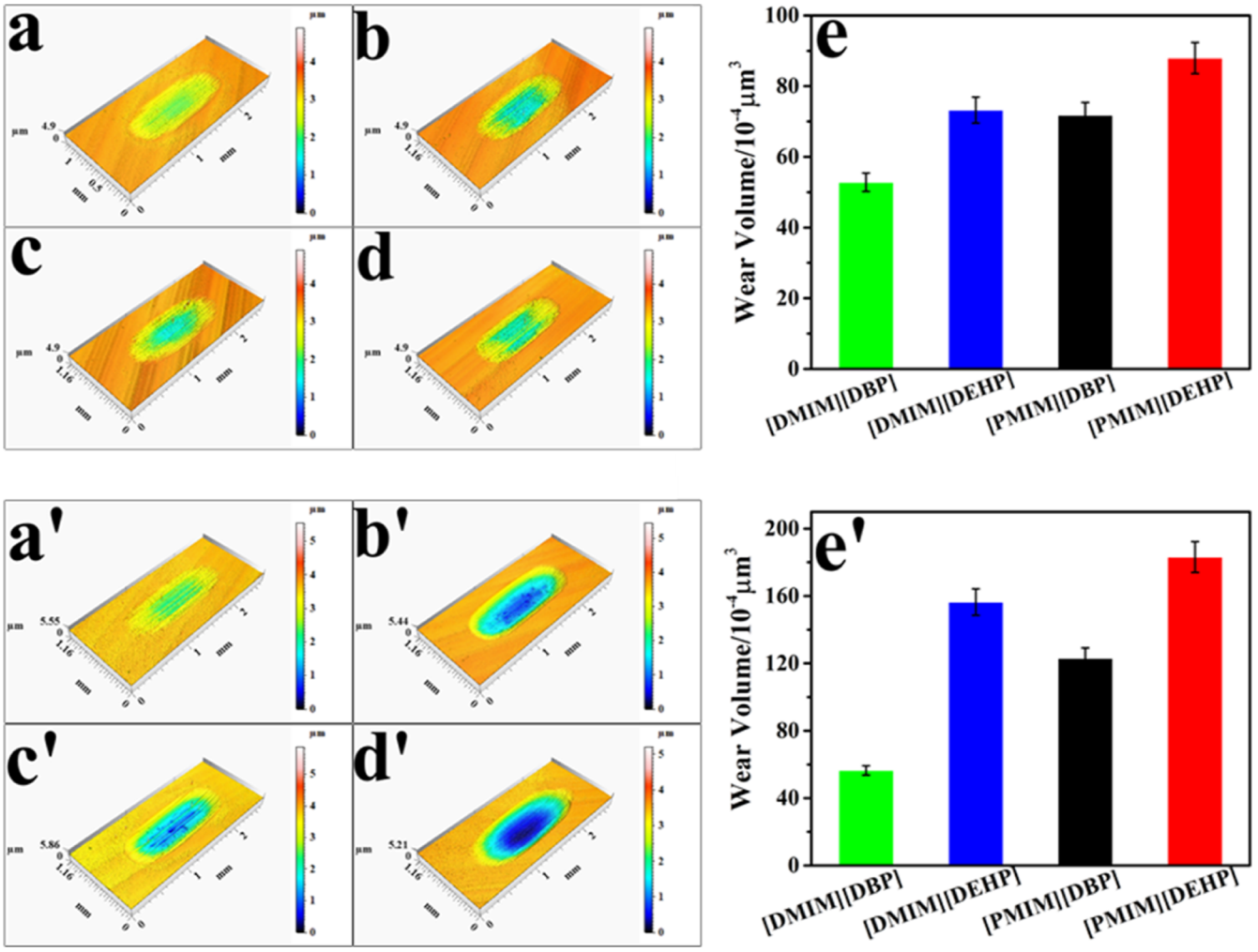

Figure 4. (a–d) and (a′–d′) wear scars lubricated by ILs under constant load and varying loads separately; (e,e′) wear volumes under constant load and varying loads, respectively.

Table 3. Wear Volumes of ILs under Constant and Varying Loads Separately

sample	[DMIM][DBP] (μm^3)	[DMIM][DEHP] (μm^3)	[PMIM][DBP] (μm^3)	[PMIM][DEHP] (μm^3)
constant load	52.8×10^{-4}	73.2×10^{-4}	71.8×10^{-4}	87.9×10^{-4}
varying load	56.5×10^{-4}	156.4×10^{-4}	123.0×10^{-4}	183.2×10^{-4}

3. RESULTS AND DISCUSSION

3.1. Tribological Test. The tribological properties of steel blocks lubricated by the four ILs were detected with the ball-on-disc SRV-IV tribotester. The friction coefficients (COFs) are shown in Figure 3a under the conditions of 300 N, 25 Hz, and RT. In the initial stage of friction, the COFs of the four ILs are relatively high (about 0.16). As the friction experiment continues, the COFs gradually decrease and tend to be stable. It is worth noting that the COFs of [DMIM][DBP] and [DMIM][DEHP] decreased to approximately 0.093 and 0.11 in the later stage of friction process. While the COFs of [PMIM][DBP] and [PMIM][DEHP] exhibit a downward

https://doi.org/10.1021/acsomega.3c01885
ACS Omega 2024, 9, 3184–3192

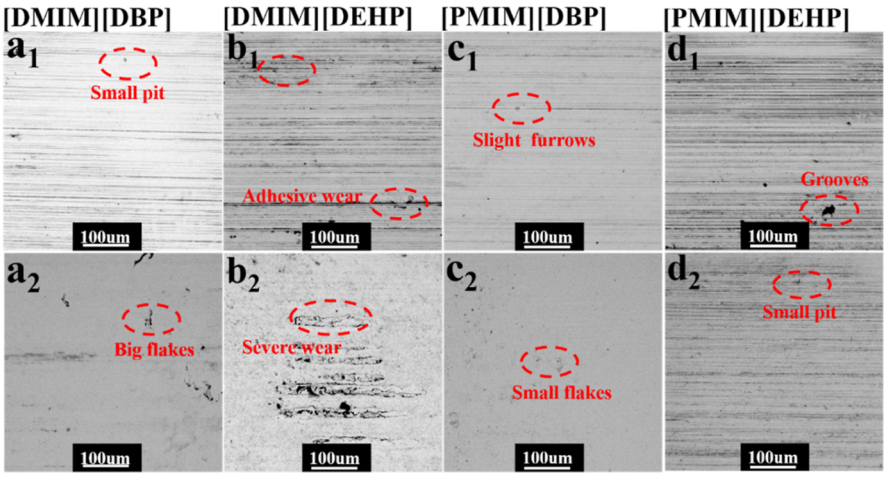

Figure 5. SEM micrographs of the wear scar surfaces under (a_1−d_1) 300 N and (a_2−d_2) varying loads.

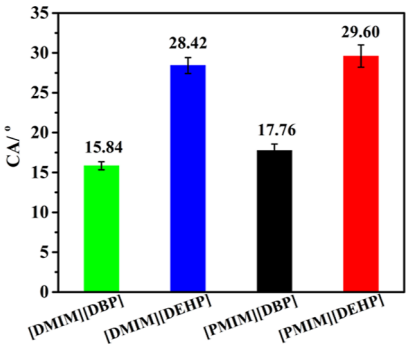

Figure 6. CAs between the four ILs and the steel blocks.

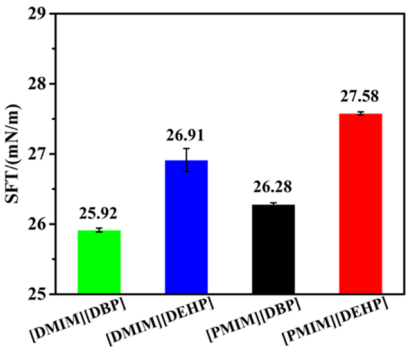

Figure 7. STFs of the four ILs.

trend during the friction process, but they are still 0.094 and 0.12. In other words, the ILs with long alkyl chain cations ([DMIM][DBP] and [DMIM][DEHP]) exhibit better anti-friction performance than the ones with short alkyl chains ([PMIM][DBP] and [PMIM][DEHP]) when they possess the same anions. Interestingly enough, comparing the COFs of the four ILs in terms of anionic alkyl length, ILs ([DMIM][DBP] and [PMIM][DBP]) with short anionic alkyl chains possess lower COFs (approximately 0.094) than the ones ([DMIM]-[DEHP] and [PMIM][DEHP]) with long anionic alkyl chains. The specific reasons will be analyzed and probed below.

Meanwhile, the tribological properties of ILs under variable load were measured as illustrated in Figure 3b. The initial load was 50 N, and it increased by 50 N every 3 min. The experiment would be stopped when the friction pair was stuck. As revealed by Figure 3b, a similar conclusion can be obtained compared with that under constant load. The tribological properties of ILs under variable loads demonstrate the same regularity as those under constant loads: [DMIM][DBP] > [PMIM][DBP] > [DMIM][DEHP] > [PMIM][DEHP]. Whenever the load increases, the COFs of ILs will undergo a sudden change, and then they will rapidly decrease and remain stable, which to some extent demonstrates that the lubricating film formed by IL is tough and stable.[20] The maximum non-seizure loads of ILs reach 450 N except for [PMIM][DBP] (400 N), indicating that all four ILs possess outstanding extreme pressure performance. When the anion contains a short alkyl chain and the cation possesses a long alkyl chain, the corresponding tribological performance is the best.

The 3D image detected by the 3D profilometer is generally utilized to determine the morphology of wear scar surface, wear depth, and corresponding wear volume.[21,22] Figure 4a−d and a′−d′, respectively, demonstrate the 3D images of the wear scars lubricated by the four ILs under constant load and varying loads. Figure 4a,a′,b,b′,c,c′,d,d′ correspond to [DMIM][DBP], [DMIM][DEHP], [PMIM][DBP], and [PMIM][DEHP], respectively. Figure 4e,e′ correspond to the calculated wear volumes, and the concrete values of ILs are demonstrated in Table 3. The wear volumes of [DMIM]-[DBP] and [PMIM][DBP] are smaller than those of [DMIM][DEHP] and [PMIM][DEHP], that is, the shorter the anionic alkyl chain length, the smaller the wear volume and the better the wear resistance. The wear volumes of [DMIM][DBP] and [DMIM][DEHP] are smaller than those of [PMIM][DBP] and [PMIM][DEHP]. The longer the cationic alkyl chain length, the greater the antiwear performance. Aforementioned results are consistent with the friction test outcomes, as illustrated in Figure 3.

3.2. Analysis of Wear Morphology of Steel Block. SEM is the commonly adopted method to detect wear marks and surface topographies. Analyzing the morphologies of wear scars can facilitate us to explain the interface behavior of lubricants during the friction process and the wear forms can be further confirmed.[23,24] Figures 5a_1−d_1 and a_2−d_2 illustrate the SEM images of the wear scars lubricated by the four ILs under constant load and varying loads, and they correspond to [DMIM][DBP], [DMIM][DEHP], [PMIM][DBP], and [PMIM][DEHP], respectively. As demonstrated in Figure 5,

https://doi.org/10.1021/acsomega.3c01885
ACS Omega 2024, 9, 3184−3192

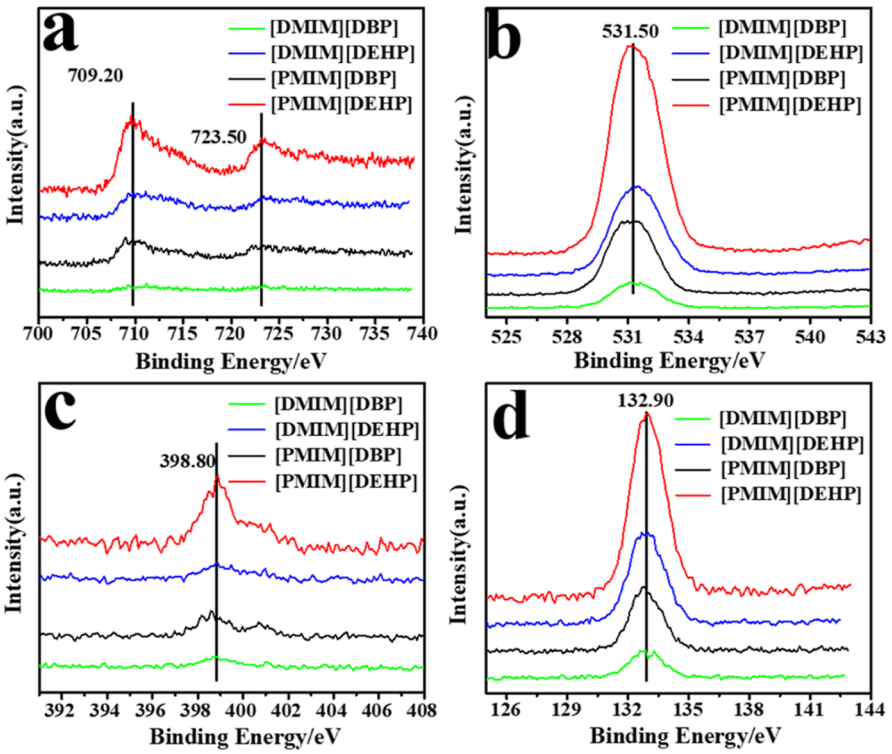

Figure 8. XPS spectra of (a) Fe 2p, (b) N 1s, (c) O 1s, and (d) P 2p of wear scar surfaces lubricated by [DMIM][DBP], [DMIM][DEHP], [PMIM][DBP], and [PMIM][DEHP], respectively, under the condition of 300 N and 25 Hz.

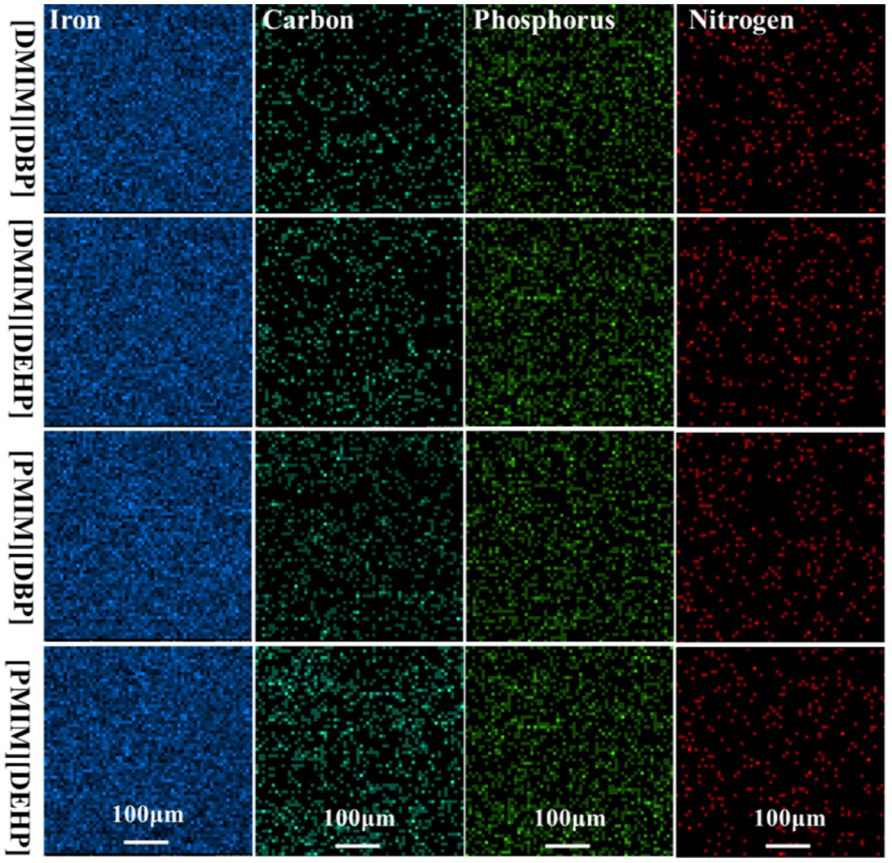

Figure 9. EDS analysis of wear scar surfaces lubricated by the four ILs.

the wear scars of Figure 5a_1,a_2,c_1,c_2 (corresponding to [DMIM][DBP] and [PMIM][DBP] separately) are relatively shallow, and the main wear form is abrasive wear. Figure 5b_1,b_2,d_1,d_2 (corresponding to [DMIM][DEHP] and

https://doi.org/10.1021/acsomega.3c01885
ACS Omega 2024, 9, 3184−3192

Table 4. Mass Contents of Wear Scar Surfaces

ILs	Fe %	C %	P %	N %
[DMIM][DBP]	70.23	29.40	0.34	0.03
[DMIM][DEHP]	69.33	30.03	0.56	0.08
[PMIM][DBP]	64.50	34.98	0.45	0.07
[PMIM][DEHP]	57.76	41.51	0.64	0.09

[PMIM][DEHP] separately) have deeper wear scars, and the main wear type is adhesive wear.

3.3. Interaction between ILs and Sliding Pair Surfaces. ILs can form highly ordered adsorption films on the surfaces of the friction pairs, which can greatly affect their tribological performance.[25] Meanwhile, the film-forming ability of ILs can be demonstrated intuitively through the measurement of their CAs. Under normal circumstances, the smaller the CA is, the faster the oil droplets spread on the surface, and the stronger the ability of the IL to form a film.[26,27] The CA measuring instrument is introduced to measure the CAs between the ILs and the steel blocks, and the corresponding testing results are depicted in Figure 6. From the figure point of view, the CA of [DMIM][DBP] (15.84°) is the smallest among the four ILs. Following [PMIM][DBP], the CA is 17.76°. The CAs of [PMIM][DEHP] and [DMIM][DEHP] are larger and they are 28.42 and 29.6°, respectively. It indicates that [DMIM][DBP] and [PMIM][DBP] comparing with [PMIM][DEHP] and [DMIM][DEHP] are more likely to form adsorption films on the friction pair surfaces. It can be attributed to that the shorter the alkyl chain length of the anion, the more negative charges it carries. Meanwhile, the metal material surfaces usually have positive charges.[28] As a result, ILs with a shorter anionic alkyl chain length possess lower CAs and they are more prone to constitute more compact adsorption films on the steel surfaces. In addition, the adsorption film formed by anions with long chain length is thicker, and this adsorption film has high compressibility and poor density and suffers from greater friction in the process of friction and wear.[29,30]

The CA of IL on the steel block surface of is often affected by the surface tension of the liquid itself.[29] To compare the adhesion of ILs on the steel block surfaces, the surface tension forces (STFs) of the four ILs were measured at RT as presented in Figure 7. Testing results manifest that it exhibits a similar law to that of the CAs. The STFs of [DMIM][DBP] and [PMIM][DBP] are less than those of [DMIM][DEHP] and [PMIM][DEHP]; that is, one IL with a shorter anionic alkyl chain length is more easily to adsorb and make up a film on the steel block surface. Meanwhile, the longer cationic alkyl chain length, the lower the SFTs in this system, manifesting that the ILs possess better adsorption capacity and film-forming ability.

3.4. Composition Analysis of Lubricating Film. *3.4.1. XPS Analysis of Worn Surfaces.* XPS can identify the element composition by measuring the binding energies between elements and determine the chemical shift of the element and judge the atomic valence.[30,31] Therefore, XPS has been diffusely adopted to detect tribo-chemical reactions in the friction process and further analyze the chemical composition of wear scar surfaces. The corresponding test results of Fe 2p, N 1s, O 1s, and P 2p are illustrated in Figure 8. The binding energies of Fe 2p are approximately 709.2 and 723.5 eV, as shown in Figure 8a, which are assigned to tough ferric oxide.[32] According to the O 1s test results (531.5 eV), it can be assigned to composite oxides (such as phosphates and oxynitrides), as depicted in Figure 8b.[33] The peaks of N 1s appear at 398.8 eV corresponding to oxynitrides and nitrogen-containing organic compounds, as described in Figure 8c. The binding energy of P 2p is approximately 132.9 eV, as represented in Figure 8d, which can be classified as iron phosphate and complex organic phosphorus compounds.[24] During the friction process, tribo-chemical reactions between the active elements (N and P) and the sliding pair surfaces occurred and a tougher wear-resistant layer was generated. Based on aforementioned experimental results, it can be concluded convincingly that the wear surface is composed of an inorganic compound film (including iron oxide, oxynitrides, and iron phosphate) and an organic boundary adsorption film. In addition, the absorption peak intensity of [PMIM][DBP] and [PMIM][DEHP] are much higher than those of [DMIM][DBP] and [DMIM][DEHP] indicating that chemical reactions are prone to occur when the ILs possess short cationic alkyl chains.

3.4.2. Energy Dispersive Spectrometry Tests of Wear Scar Surfaces. When the contact load reaches several hundred Newtons, the pressure between the sliding pairs can reach the order of 10^6 Pa. In such a harsh environment, tribo-chemical reactions are prone to occur between ILs and friction pair surfaces.[16] EDS is often introduced to detect the tribo-chemical products and element contents.[34] Figure 9 provides the element distribution of iron, carbon, nitrogen, and phosphorus on the wear scar surfaces. The occurrence of C, N, and P on the wear scar surfaces indicates the occurrence of tribo-chemical reactions during the friction process. To further verify the intensity of the tribo-chemical reactions, EDS analysis was performed to probe the wear scars lubricated by the four ILs, and the statistical results are illustrated in Table 4. Comparing the test results, the wear scar surfaces lubricated by [DMIM][DEHP] and [PMIM][DEHP] contain higher contents of nitrogen and phosphorous than those lubricated by [DMIM][DBP] and [PMIM][DBP]. Meanwhile, the carbon content of wear scar surfaces increases significantly with the reduction of cationic alkyl chain lengths and the

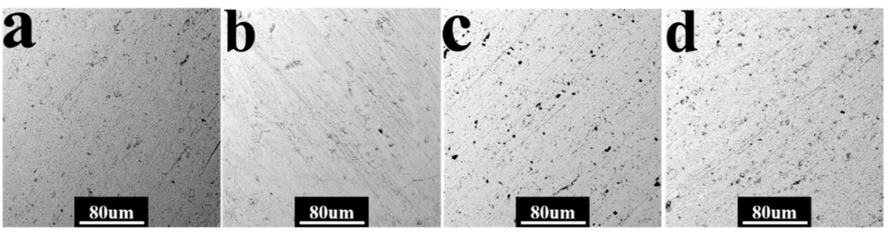

Figure 10. SEM images of the copper block surfaces after corrosion treatments: (a) [DMIM][DBP], (b) [DMIM][DEHP], (c) [PMIM][DBP], and (d) [PMIM][DEHP].

https://doi.org/10.1021/acsomega.3c01885
ACS Omega 2024, 9, 3184−3192

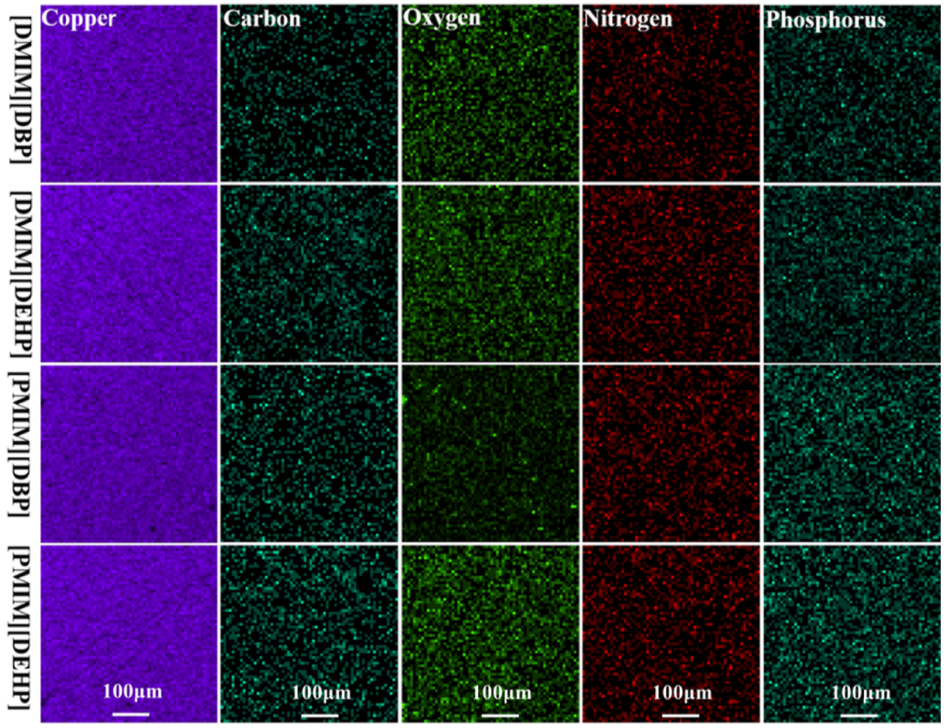

Figure 11. EDS analysis of the copper block surfaces after the corrosion treatments.

Table 5. Element Composition of the Copper Block Surfaces after Corrosion Treatments

ILs	Cu wt %	C wt %	O wt %	N wt %	P wt %
[DMIM][DBP]	85.98	10.02	3.08	0.62	0.10
[DMIM][DEHP]	78.71	16.12	3.95	1.09	0.13
[PMIM][DBP]	84.91	10.35	3.81	0.78	0.14
[PMIM][DEHP]	79.01	14.56	3.72	2.61	0.09

increase of anionic alkyl chain lengths. These results suggest that violent tribo−chemical reactions are more likely to occur between [DEHP]-based ILs and the friction pair surfaces, and the severe tribo-chemical reactions will accelerate the wear of sliding pairs.

3.4.3. Corrosion Tests of ILs. The corrosion property can reflect the adsorption capacity of the IL on the substrate surface and the degree of the chemical reaction.[35,36] Based on this, the copper blocks were immersed in the four ILs, respectively. To better simulate the severe thermal effect during the friction process, the copper blocks and the ILs were placed in an oven at 200 °C for 2 h.[37,38] The corresponding corrosion treatment results of steel blocks are illustrated in Figures S2 and S3. Figure 10 demonstrates the SEM of the copper block surfaces after the corrosion treatment. At 200 °C, all four ILs were decomposed (mainly the decomposition of the imidazole group) and rapidly underwent chemical reactions with the copper block surfaces. The corrosion of [DMIM][DBP] and [PMIM][DBP] is relatively light, with only partial pitting as exhibited in Figure 10a,c. The corrosion morphology of [DMIM][DEHP] contains pitting and pits, and the degree of corrosion is more serious than those of the previous two, as manifested in Figure 10b. [PMIM][DEHP] displays the most severe corrosion, and large areas of corrosion pits appear as illustrated in Figure 10d. Above results reveal that ILs with short anionic alkyl chains possess a strong film-forming ability and low corrosiveness.

Subsequently, EDS measurements were carried out to analyze the corrosion degree and element composition of the copper block surfaces, and the corresponding test results are illustrated in Figure 11 and Table 5. Through further elemental analysis of the copper block surfaces, it can be detected that the surfaces of copper blocks soaked in the ILs with longer anionic alkyl chains possessed more nitrogen and phosphorus elements. Meanwhile, it can also be perceived in more detail that the ILs exhibit weak corrosion property with the increase of cationic alkyl chains when they possess the same anions. It is generally known that the occurrence of corrosion will result in corrosion wear and aggravate the wear of sliding pairs in the process of friction. The corrosion test results can give a good interpretation to the tribological performance of the four ILs. The longer the anionic alkyl chain, the more serious the corrosion of the sliding pair. The most immediate effect of corrosion is to increase the roughness of the material surface. In general, the rougher the surface of the material, the more severe the wear of the sliding pair in the process of friction. The corrosion test results can give a good interpretation to the tribological performance of the four ILs.

4. CONCLUSIONS

In summary, four imidazole-based phosphate ILs were synthesized and their tribological properties for steel−steel sliding friction pairs were evaluated. Tribological test results indicate that the ILs with longer cationic alkyl chain lengths and shorter anionic alkyl chain lengths exhibit better tribological performance. And anions have a greater impact on the tribological properties of ILs. To further explore the intrinsic mechanism of aforementioned results, various characterization methods and testing techniques are employed. The reasons for aforementioned results can be attributed to two aspects. For one thing, ILs with shorter anionic alkyl chain possess higher charge density and are more prone to form

https://doi.org/10.1021/acsomega.3c01885
ACS Omega 2024, 9, 3184−3192

more compact and steady adsorption film on the friction pair surfaces. Meanwhile, ILs with longer cationic alkyl chain have milder tribo-chemical reactions with the steel surfaces, which can effectively enhance the tribological performance and reduce the corrosion wear during the friction process. Combining the above-mentioned two factors, the imidazole phosphate ILs with long cationic alkyl chain and short anionic alkyl chain possess good tribological properties.

■ ASSOCIATED CONTENT

Supporting Information

The Supporting Information is available free of charge at https://pubs.acs.org/doi/10.1021/acsomega.3c01885.

Structural characterization of the ILs by FT-IR and NMR, water content measurements of ILs, and SEM images and EDS analysis of the steel block surfaces after corrosion treatments (PDF)

■ AUTHOR INFORMATION

Corresponding Author

Guowei Huang − *State Key Laboratory of Advanced Processing and Recycling of Nonferrous Metals, Lanzhou University of Technology, 730050 Lanzhou, Gansu, P. R. China;* orcid.org/0000-0002-1555-7552; Email: huang_guow@163.com

Authors

Li Sun − *State Key Laboratory of Advanced Processing and Recycling of Nonferrous Metals, Lanzhou University of Technology, 730050 Lanzhou, Gansu, P. R. China*

Luxing Li − *State Key Laboratory of Advanced Processing and Recycling of Nonferrous Metals, Lanzhou University of Technology, 730050 Lanzhou, Gansu, P. R. China*

Linlu Pei − *State Key Laboratory of Advanced Processing and Recycling of Nonferrous Metals, Lanzhou University of Technology, 730050 Lanzhou, Gansu, P. R. China*

Wangle Xue − *State Key Laboratory of Advanced Processing and Recycling of Nonferrous Metals, Lanzhou University of Technology, 730050 Lanzhou, Gansu, P. R. China*

Ruichao Wang − *State Key Laboratory of Advanced Processing and Recycling of Nonferrous Metals, Lanzhou University of Technology, 730050 Lanzhou, Gansu, P. R. China*

Yifei Wang − *Dulwich International High School Zhuhai, 519060 Zhuhai, Guangdong, P. R. China*

Complete contact information is available at: https://pubs.acs.org/10.1021/acsomega.3c01885

Notes

The authors declare no competing financial interest.

■ ACKNOWLEDGMENTS

The authors are grateful for the financial support from National Natural Science Foundation of China (52005235), the Hongliu Distinguished Young Talent Support Program of Lanzhou University of Technology, Youth science and technology talent lifting project of Gansu Province (GXH2021061108), and Natural Science Foundation of Gansu Province (20JR5RA454).

■ REFERENCES

(1) He, X.; Meyer, H. M.; Luo, H.; Qu, J. Wear penalty for steel rubbing against hard coatings in reactive lubricants due to tribochemical interactions. *Tribol. Int.* **2021**, *160*, 107010.

(2) Desanker, M.; He, X.; Lu, J.; Liu, P.; Pickens, D. B.; Delferro, M.; Marks, T. J.; Chung, Y. W.; Wang, Q. J. Alkyl-cyclens as effective sulfur- and phosphorus-free friction modifiers for boundary lubrication. *ACS Appl. Mater. Interfaces* **2017**, *9*, 9118−9125.

(3) Zhang, Y.; Zhu, H.; Ji, Z.; Cheng, Y.; Zheng, L.; Wang, L.; Li, X. Experiments and kinetic modeling of fructose dehydration to 5-hydroxymethylfurfural with hydrochloric acid in acetone−water solvent. *Ind. Eng. Chem. Res.* **2022**, *61*, 13877−13885.

(4) Ye, C.; Liu, W.; Chen, Y.; Yu, L. Room-temperature ionic liquids: a novel versatile lubricant. *Chem. Commun.* **2001**, 2244−2245.

(5) Oh, S.; Keating, M. J.; Biddinger, E. J. Physical and electrochemical properties of ionic-liquid- and ester-based cosolvent mixtures with lithium salts. *Ind. Eng. Chem. Res.* **2022**, *61*, 12118−12131.

(6) Al Kaisy, G. M. J.; Mutalib, M. I. A.; Rao, T. V. V. L. N.; Senatore, A. Tribological performance of low viscosity halogen-free ammonium based protic ionic liquids with carboxylate anions as neat lubricants. *Tribol. Int.* **2021**, *160*, 107058.

(7) Stump, B. C.; Zhou, Y.; Luo, H.; Leonard, D. N.; Viola, M. B.; Qu, J. New functionality of ionic liquids as lubricant additives: mitigating rolling contact fatigue. *ACS Appl. Mater. Interfaces* **2019**, *11*, 30484−30492.

(8) Zhang, J.; Jiang, Y.; Gao, Y.; Li, J. Tribological properties of cholesteric fluorinated liquid crystal as lubricant additives in PAO4 under elevated temperatures. *Ind. Eng. Chem. Res.* **2021**, *60*, 8127−8138.

(9) Zhou, Y.; Qu, J. Ionic liquids as lubricant additives: a review. *ACS Appl. Mater. Interfaces* **2017**, *9*, 3209−3222.

(10) Donato, M. T.; Colaço, R.; Branco, L. C.; Saramago, B. A review on alternative lubricants: Ionic liquids as additives and deep eutectic solvents. *J. Mol. Liq.* **2021**, *333*, 116004.

(11) Qu, J.; Bansal, D. G.; Yu, B.; Howe, J. Y.; Luo, H.; Dai, S.; Li, H.; Blau, P. J.; Bunting, B. G.; Mordukhovich, G.; Smolenski, D. J. Antiwear performance and mechanism of an oil-miscible ionic liquid as a lubricant additive. *ACS Appl. Mater. Interfaces* **2012**, *4*, 997−1002.

(12) Guo, Y.; Qiao, D.; Han, Y.; Zhang, L.; Feng, D.; Shi, L. Application of alkylphosphate ionic liquids as lubricants for ceramic material. *Ind. Eng. Chem. Res.* **2015**, *54*, 12813−12825.

(13) Zheng, Z.; Yu, H.; Chen, H.; Liu, X.; Wang, H.; Feng, D.; Qiao, D. Guanidine-phosphate ionic liquids as antiwear additives in two basic oils: different lubrication mechanisms. *Tribol. Int.* **2021**, *160*, 106942.

(14) Sharma, V.; Gabler, C.; Doerr, N.; Aswath, P. B. Mechanism of tribofilm formation with P and S containing ionic liquids. *Tribol. Int.* **2015**, *92*, 353−364.

(15) Gusain, R.; Dhingra, S.; Khatri, O. P. Fatty-acid-constituted halogen-free ionic liquids as renewable, environmentally friendly, and high-performance lubricant additives. *Ind. Eng. Chem. Res.* **2016**, *55*, 856−865.

(16) Tantardini, C.; Oganov, A. R. Thermochemical electronegativities of the elements. *Nat. Commun.* **2021**, *12*, 2087.

(17) Huang, G.; Fan, S.; Ba, Z.; Cai, M.; Qiao, D. Insight into the lubricating mechanism for alkylimidazolium phosphate ionic liquids with different alkyl chain length. *Tribol. Int.* **2019**, *140*, 105886.

(18) Pejaković, V.; Tomastik, C.; Dörr, N.; Kalin, M. Influence of concentration and anion alkyl chain length on tribological properties of imidazolium sulfate ionic liquids as additives to glycerol in steel-steel contact lubrication. *Tribol. Int.* **2016**, *97*, 234−243.

(19) Parrish, J. P.; Salvatore, R. N.; Jung, K. W. Perspectives on alkyl carbonates in organic synthesis. *Tetrahedron* **2000**, *56*, 8207−8237.

(20) Sharma, V.; Doerr, N.; Aswath, P. B. Chemical-mechanical properties of tribofilms and their relationship to ionic liquid chemistry. *RSC Adv.* **2016**, *6*, 22341−22356.

(21) Shi, R.; Wang, B.; Yan, Z.; Wang, Z.; Dong, L. Effect of surface topography parameters on friction and wear of random rough surface. *Materials* **2019**, *12*, 2762.
(22) He, J.; Cao, Y.; Li, Z.; Wang, Y. Study of tribological properties of polymer derived ZrB2-SiC ceramics. *Ceram. Int.* **2018**, *44*, 15627−15630.
(23) Cai, M.; Liang, Y.; Zhou, F.; Liu, W. Anticorrosion imidazolium ionic liquids as the additive in poly(ethylene glycol) for steel/Cu-Sn alloy contacts. *Faraday Discuss.* **2012**, *156*, 147−157.
(24) Huang, G.; Yu, Q.; Ma, Z.; Cai, M.; Liu, W. Probing the lubricating mechanism of oil-soluble ionic liquids additives. *Tribol. Int.* **2017**, *107*, 152−162.
(25) Qu, J.; Truhan, J. J.; Dai, S.; Luo, H.; Blau, P. J. Ionic liquids with ammonium cations as lubricants or additives. *Tribol. Lett.* **2006**, *22*, 207−214.
(26) Ismail, M. F.; Khorshidi, B.; Sadrzadeh, M. New insights into the prediction of adaptive wetting of a solid surface under a liquid medium. *Appl. Surf. Sci.* **2020**, *532*, 147444.
(27) Kirk, S.; Strobel, M.; Lyons, C. S.; Janis, S. A statistical comparison of contact angle measurement methods. *J. Adhes. Sci. Technol.* **2019**, *33*, 1758−1769.
(28) Li, Z.; Mangolini, F. Recent advances in nanotribology of ionic liquids. *Exp. Mech.* **2021**, *61*, 1093−1107.
(29) Di Lecce, S.; Kornyshev, A. A.; Urbakh, M.; Bresme, F. Lateral Ordering in Nanoscale Ionic Liquid Films between Charged Surfaces Enhances Lubricity. *ACS Nano* **2020**, *14*, 13256−13267.
(30) Bresme, F.; Kornyshev, A. A.; Perkin, S.; Urbakh, M. Electrotunable friction with ionic liquid lubricants. *Nat. Mater.* **2022**, *21*, 848−858.
(31) Novák, V.; Řehácková, L.; Váňová, P.; Smetana, B.; Konecná, K.; Drozdová, L.; Rosypalová, S. Surface and interfacial properties of Fe-C-O-Cr alloys in contact with alumina. *J. Min. Metall., Sect. B* **2020**, *56*, 143−151.
(32) Huang, G.; Yu, Q.; Cai, M.; Zhou, F.; Liu, W. Investigation of the lubricity and antiwear behavior of guanidinium ionic liquids at high temperature. *Tribol. Int.* **2017**, *114*, 65−76.
(33) Huang, G. H.; Sun, Z. L.; Li, H. J.; Feng, D. F. Rho GTPase-activating proteins: regulators of Rho GTPase activity in neuronal development and CNS diseases. *Mol. Cell. Neurosci.* **2017**, *80*, 18−31.
(34) Cai, M.; Liang, Y.; Zhou, F.; Liu, W. A novel imidazolium salt with antioxidation and anticorrosion dual functionalities as the additive in poly(ethylene glycol) for steel/steel contacts. *Wear* **2013**, *306*, 197−208.
(35) Fan, M.; Liang, Y.; Zhou, F.; Liu, W. Dramatically improved friction reduction and wear resistance by in situ formed ionic liquids. *RSC Adv.* **2012**, *2*, 6824.
(36) Jiménez, A. E.; Bermúdez, M. D. Ionic liquids as lubricants of titanium-steel contact. Part 2: friction.; wear and surface interactions at high temperature. *Tribol. Lett.* **2009**, *37*, 431−443.
(37) Zhang, Y.; Forsyth, M.; Hinton, B. R. The effect of treatment temperature on corrosion resistance and hydrophilicity of an ionic liquid coating for Mg-based stents. *ACS Appl. Mater. Interfaces* **2014**, *6*, 18989−18997.
(38) Huang, G.; Yu, Q.; Ma, Z.; Cai, M.; Zhou, F.; Liu, W. Oil-soluble ionic liquids as antiwear and extreme pressure additives in poly-α-olefin for steel/steel contacts. *Friction* **2017**, *7*, 18−31.

https://doi.org/10.1021/acsomega.3c01885
ACS Omega 2024, 9, 3184−3192